

## **Mathematic Simulation on the Coordinated Forces Exerted on In-Service Joint Supports**

\*Huayou Liang, \*\*Haiqing Zhou, \*\*\*Shuling Zhou, \*\*\*\*Jianqing Li

\* Dept. of Civil Engineering, Logistical Engineering University,  
Chongqing, China (964493929@qq.com)

\*\* Dept. of Civil Engineering, Logistical Engineering University,  
Chongqing, China ([zhou-haiqing@163.com](mailto:zhou-haiqing@163.com))

\*\*\* The 4th Engineering Design & Research Academy General Staff PLA, Beijing, China.

\*\*\*\* Dept. of National Defense Architecture Planning & Environmental Engineering,  
Logistical Engineering University, Chongqing, China.

### **Abstract**

FLAC3D was adopted to mathematically simulate a multi-stage slope with joint supports of anchor cable frames and anti-slide piles. The simulation aims to discuss the change law of axial forces of cable anchors in the multi-stage slope whose upper part is under the action of evenly distributed loads. The research result shows that: When evenly distributed load is exerted on the top of a slope with in-service joint support, slope slide mass will slide along the sliding surface as a block, the growth rate of 3# cable anchor is higher than that of 2# cable anchor, and the 1# cable anchor has the lowest growth rate among them; the growth rate of 4# cable anchor is similar to the one of 5# cable anchor, and the 6# cable anchor has a much faster growth rate by comparison, it is the cable-anchor-mounted anti-slide pile and the tier-two anchor cable frame that bear most of the landslide thrust.

### **Key words**

Joint support, axial forces of cable anchors, slope

### **1. Introduction**

Anchor cable frames and anti-slide piles (including anchor-cable-mounted anti-slide piles) are two effective support structures for slope reinforcement and landslide control<sup>[1-3]</sup>. However, for some high slopes and/or huge landslide control engineering, the use of any single support fails to counteract tremendous landslide thrust. To resist landslide thrust, a common support adopted in such engineering work in China is the joint support of anchor cable frames and anti-slide piles<sup>[4]</sup>.

For many years, the joint support has been successfully applied to landslide control and slope support, addressing plenty of problems in slope stabilization<sup>[4-6]</sup>. Despite the abundant engineering experience, most theoretical studies on joint support design and its calculation are still imperfect<sup>[7-9]</sup>. This is a typical phenomenon that theoretical research lags behind corresponding engineering practice. Given this, it is a must that such research is established on the basis of forces exerted on the joint support throughout its service time<sup>[10-12]</sup>.

The most perilous slope state for the majority of slope support projects does not occur during the construction<sup>[13-16]</sup>, but in the process of using the support instead. The change of external conditions leads to the change of landslide thrust, which breaks the balance of internal stresses of rock soil. The ever-varying landslide thrust is likely to be distributed to all levels of support structures in a specific way, and a certain level of support structure perhaps consequentially bear more landslide forces than its maximum limit, which is the reason why a slope becomes unstable even with the occurrence of landslide. The exertion of evenly distributed loading on a slope top is a frequent working conditions. The paper discussed the change law of axial forces of each cable anchor in a high, multi-stage slope whose upper part is under the action of evenly distributed loads. The research result lays foundation for theoretical research into the design and calculation of joint supports.

## **2. Numerical model:**

### **2.1. Establishment of the model**

FLAC3D was used to build up a 3D finite element model for a tri-stage slope, as shown in Figure 1. The slope size is 50m×7m×30m. There is a total of 45,864 entity units and 51,272 nodes for the slope. Vertical displacement constraints were placed on the bottom plane of the model, and horizontal displacement constraints on the planes of X=0、X=50 and Y=0、Y=7. The plane of Z=30 is a free plane. Figure 2 is the finite element model for the slope and its support after the completion of slope construction, containing two tiers of anchor cable frames and a cable-anchor-mounted anti-slide pile.

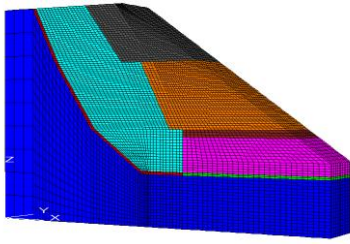


Figure 1. The 3D finite element model for a tri-stage slope

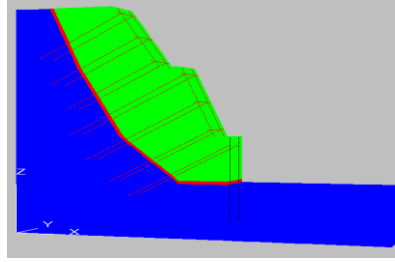


Figure 2. The finite element model for the slope and its support after the completion of slope construction

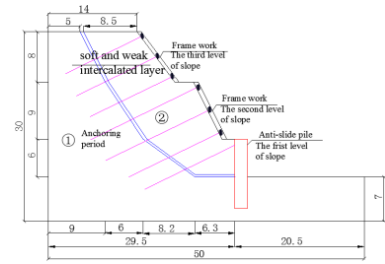


Figure 3. The diagram for the cross section of the slope and its support

## 2.2 Model parameters

The research objective is a typical rock-soil compound slope with a soft and weak intercalated layer as thick as 0.5m. Figure 3 is the diagram for the cross section of the slope and its support, where ① represents the bed rock and ② is the soil slide. For the third tier of this tri-tier slope, the slope rate upon excavation is 1:0.75, the excavation height is 8m, and the platform is as wide as 2m. The respective parameters for the second tier are 1:0.5, 9m, and 1m. The excavation height for the first tier is 6m. The Mohr-Coulomb elastic-plastic model in FLAC3D is employed in the paper, because it complies with the non-associated flow principle, which is accordingly well adaptive to the real situations of the tri-tier slope. Table 1 shows the mechanical parameters of rock-soil mass at all levels. Figure 3 is the slope support structure, where the last two tiers are supported by prestressed anchor cable frames and the first tier is supported by prestressed cable anchor anti-slide piles.

The anchoring cable frame is constructed with the cable anchor unit and beam unit in FLAC3D. Each plane is designed to be supported by 3 lateral beams and 2 longitudinal beams, all of which are 300 mm×300 mm. Beams in the same direction are at the uniform interval of 4m, and the horizontal tilting angle of all cable anchors is 26°. The lengths of the anchoring section for the second tier and third tier are 7m and 5m, respectively. Cable anchor anti-slide piles are used to support the first tier, whose parameters are: the total pile length 11m, the length of the anchoring section 5m, the cross section of the pile body 1 m×1 m, the pile interval 4m, the distance of the cable anchor from the pile top 1m, and the horizontal tilting angle of the cable anchor 26°. Table 2 is the calculation parameters for the cable anchor. Table 3 shows the calculation parameters for frame beams. Table 4 is the calculation parameters for the anti-slide pile.

Tab 1. Mechanical parameters of rock soil mass

Slope body	Unit weight (/kN/m <sup>3</sup> )	Cohesion /kPa	Internal friction angle/(°)	Elastic modulus/MPa
Bed rock	21.5	708	31.3	980
Slide mass	17	34.6	24.6	200
Soft and weak intercalated layer	17	17.3	12.55	200

Tab 2. Parameters of cable anchors

Parameter	Elastic modulus /Gpa	Cross section /m <sup>2</sup>	Friction angle of the cement paste/(°)	Cohesive force of the cement paste at unit length/(kN • m <sup>-1</sup> )	Stiffness of the cement paste at unit length /GPa	The total perimeter of the cement/m
Free section	195	$5.56 \times 10^{-4}$	0	0	0	0
Anchoring section	195	$5.56 \times 10^{-4}$	25	$2.1 \times 10^3$	0.56	0.408 2

Tab 3. Parameters of frame beams

Elastic modulus /GPa	Poisson's ratio	Cross section /m <sup>2</sup>	Inertia moment of axis y /m <sup>4</sup>	Inertia moment of axis z /m <sup>4</sup>	Polar moment of inertia /m <sup>4</sup>
28	0.2	0.09	$6.75 \times 10^{-4}$	$6.75 \times 10^{-4}$	$1.35 \times 10^{-3}$

Tab.4. Parameters of anti-sliding piles

Elastic modulus /GPa	Poisson's ratio	Internal force of normal coupling springs /(kN • m <sup>-1</sup> )	Friction angle of normal coupling springs /(°)	Stiffness of normal coupling springs at unit length /GPa	Internal force of shear coupling springs /(kN • m <sup>-1</sup> )	Friction angle of shear coupling springs /(°)	Stiffness of shear coupling springs at unit length/GPa
----------------------------	--------------------	--	---	---	--	---	---

### 3. Simulation method

Generally, when calculating the thrust of an arbitrary landslide by use of the transfer coefficient method, sliding surface of the landslide is simplified as a fold line, as shown in Figure 4. According to the transfer coefficient method, the  $i$ th block is isolated from the whole surface, and all forces exerted on the slope surface are resolved into components along the corresponding directions of the block, which is demonstrated in Figure 5. The given safety coefficient falls within 1.05-1.25. The remainder of landslide thrust of the  $i$ th block is

$$E_i = K_s W_i \sin \theta_i - W_i \cos \theta_i - c_i l_i + \psi_i E_{i-1} \quad (1)$$

Where  $E_i$  denotes the remainder of sliding force of the  $i$ th block;  $E_{i-1}$  is the remainder of sliding force of the  $i-1$  th block;  $W_i$  is the weight of the  $i$ th block;  $N_i$ ,  $S_i$  are the respective sliding counterforce of the  $i$ th block;  $\psi_i$  is the transmission coefficient,  $\psi_i = \cos(\theta_{i-1} - \theta_i) - \sin(\theta_{i-1} - \theta_i) \tan \varphi_i$ ;  $c_i$  is the cohesive force of rock soil mass on the sliding surface of the  $i$ th block;  $l_i$  is the sliding length of the  $i$ th block;  $\varphi_i$  is the internal friction angle of the rock soil mass on the sliding surface of the  $i$ th block; and  $\theta_i$  is the tilting angle of the sliding surface of the  $i$ th block. When the joint support is in service, there are usually heap loads or other loads acting on the slope top. According to calculation formula (1), when the slope top is under the action of evenly distributed loads (Figure 6), the landslide thrust will increase with the increase of forces exerted on slope tops. The original equilibrium of forces is then broken. The increment of landslide thrust is likely to be distributed to all levels of support structures according to a specific law. During construction, the supports of all the slope tiers are under the action of 800kN prestress. When all the excavation and reinforcement work are done, an evenly distributed gradual loading is exerted on the place 5-14m higher above the slope top, which begins at  $1 \times 10^4$  N and increases at each interval of  $1 \times 10^4$  N. During the calculation by the mathematical model, the his sel cab force instruction in FLAC3D is executed by recording the change of prestress acted on cable anchors in each tier of supports. As the supports are symmetric, according to the said simulation result, the axial stresses of a pair of symmetric cable anchors in supports are the same. Given this, the paper only discusses the change law of the axial stress of a cable anchor on one side. As a matter of convenience, the paper numbers the cable anchors as 1#~7# from top to down (Figure 6).

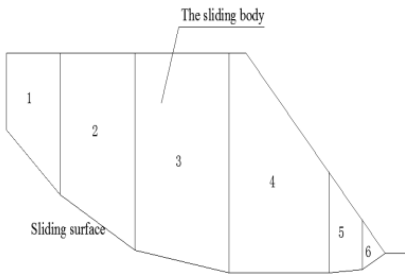


Figure 4. The fold line type sliding surface of the landslide

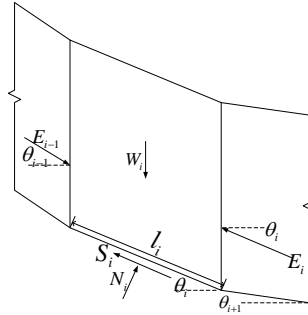


Figure 5. Forces exerted on the  $i$ th block

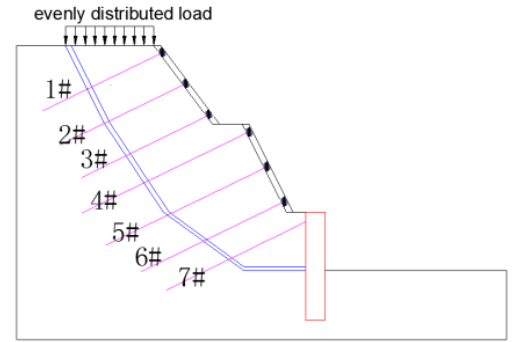


Figure 6. The diagram of evenly distributed loads and cable anchor No.

## 4. Simulation result analysis

After simulating slope excavation and support construction, we exerted different loads of even distribution on the top of the slope slide, and recorded the change of axial forces acted on cable anchors in each tier of supports. The simulation result can be used to obtain the change law of axial stresses of cable anchors when the supports are under the action of different loads.

### 4.1. The change law of axial stresses of cable anchors for tier-three slope support

Figure 8-10 are the cloud maps of the maximum displacement, the horizontal displacement and the vertical displacement, respectively, of the tier-three slope when the evenly distributed load exerted on the slope top is  $4 \times 10^4$  N. Figure 7 displays the law for the axial stress of cable anchors in tier-three slope support to change with the change of the evenly distributed load. As can be seen from Figure 8-10, when there are evenly distributed loads exerted on the slope top, the tier-three slope body will move along the sliding surface as the landslide thrust increases, in the form of block movement. Through theoretical analysis, it is ascertained that the finished support structure integrates with the slope body as a whole, as such the former slides together with the movement of the slope body.

However, constrained by the anchoring section of the prestressed cable anchor, the axial stress of the cable anchor will negatively increase so as to realize a new balance between itself and the reinforced landslide thrust. According to Figure 7, when the evenly distributed load is limited to a certain value range, the axial stress of the cable anchor barely vary; as the load increases, the axial stress of the cable anchor in the tier-three slope support gradually increases accordingly. The axial stress and the load are not linearly correlated with each other. The growth rate of 3# cable anchor exceeds that of 2# cable anchor, and the 1# cable anchor has the lowest growth rate. According to

Figure 9, the horizontal displacement of the tier-three slope support witness a gradual top-to-down rise. The fact that the contour line of the horizontal displacement is inclined demonstrates that upon the exertion of the evenly distributed load on the slope top, the tier-three slope and the frame beam will rotate counterclockwise during their sliding process.

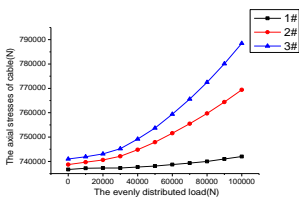


Figure 7. The axial force exerted on the cable anchors in the tier-three slope

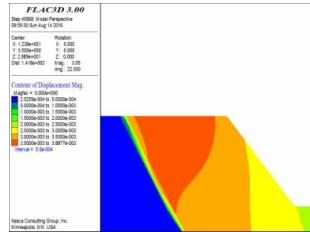


Figure 8. The cloud map of the maximum displacement of the tier-three slope when the evenly distributed load exerted on the slope top is  $4 \times 10^4$  N

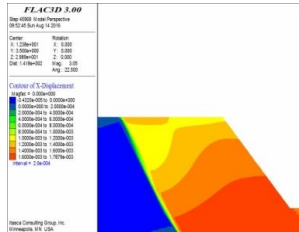


Figure 9. The cloud map of the horizontal displacement of the tier-three slope when the evenly distributed load exerted on the slope top is  $4 \times 10^4$  N

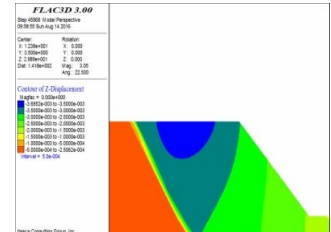


Figure 10. The cloud map of the vertical displacement of the tier-three slope when the evenly distributed load exerted on the slope top is  $4 \times 10^4$  N

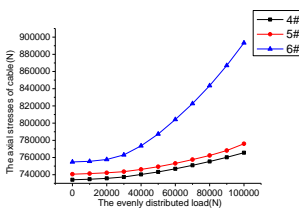


Figure 11. The axial force exerted on the cable anchors in the tier-two slope

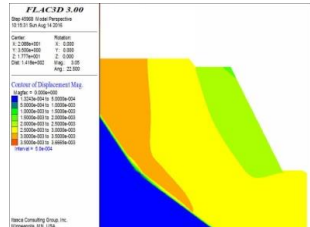


Figure 12. The cloud map of the maximum displacement of the tier-two slope when the evenly distributed load exerted on the slope top is  $4 \times 10^4$  N

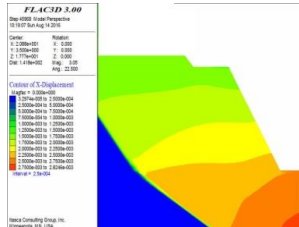


Figure 13. The cloud map of the horizontal displacement of the tier-two slope when the evenly distributed load exerted on the slope top is  $4 \times 10^4$  N

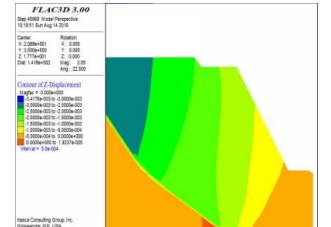


Figure 14. The cloud map of the vertical displacement of the tier-two slope when the evenly distributed load exerted on the slope top is  $4 \times 10^4$  N

## 4.2. The change law of axial stresses of cable anchors for tier-two slope support

Figure 12-14 are the cloud maps of the maximum displacement, the horizontal displacement and the vertical displacement, respectively, of the tier-two slope when the evenly distributed load exerted on the slope top is  $4 \times 10^4$  N. Figure 11 displays the law for the axial stress of cable anchors in tier-two slope support to change with the change of the evenly distributed load. As can be seen from Figure 12-14, when there are evenly distributed loads exerted on the slope top, the tier-two slope body will move along the sliding surface as the landslide thrust increases, in the form of block movement. Constrained by the anchor cable frames, the displacement of tier-two slope gradually decreases from the sliding surface to the free face. According to Figure 11, when the evenly distributed load is limited to a certain value range, the axial stress of the cable anchor barely vary; as the load increases, the axial stress of the cable anchor in the tier-two slope support gradually increases accordingly. There are non-linear relationships between the axial stress and the load. The growth rate of 4# cable anchor is similar to the one of 5# cable anchor, and the 6# cable anchor has a much faster growth rate by comparison. According to Figure 13, the contour line of the horizontal displacement is almost straight, which demonstrates that upon the exertion of the evenly distributed load on the slope top, the tier-two slope barely rotates counterclockwise during its sliding process.

## 4.3. The change law of axial stresses of cable anchors for tier-one slope support

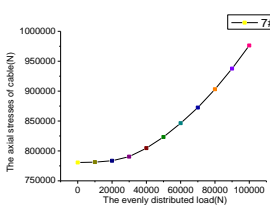


Figure 15. The axial force exerted on the cable anchors in the tier-one slope

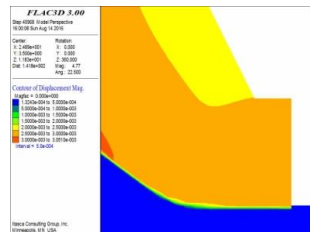


Figure 16. The cloud map of the maximum displacement of the tier-one slope when the evenly distributed load exerted on the slope top is  $4 \times 10^4$  N

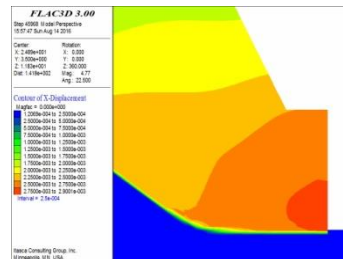


Figure 17. The cloud map of the horizontal displacement of the tier-one slope when the evenly distributed load exerted on the slope top is  $4 \times 10^4$  N

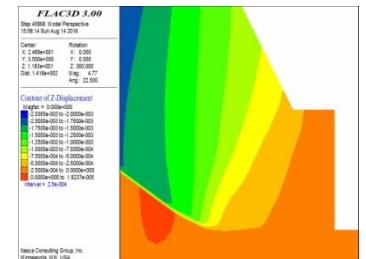


Figure 18. The cloud map of the vertical displacement of the tier-one slope when the evenly distributed load exerted on the slope top is  $4 \times 10^4$  N

Figure 16-18 are the cloud maps of the maximum displacement, the horizontal displacement and the vertical displacement, respectively, of the tier-one slope when the evenly distributed load exerted on the slope top is  $4 \times 10^4$  N. Figure 15 displays the law for the axial stress of cable anchors

in tier-one slope support to change with the change of the evenly distributed load. As can be seen from Figure 16-18, the tier-one slope slides along the sliding surface as a whole. Due to the influence of the cable anchor in the anti-slide pile, the horizontal displacement in the vicinity of the anchoring point is smaller than that of any other points. According to Figure 15, when the evenly distributed load is limited to a certain value range, the axial stress of the cable anchor barely vary; as the load increases, the axial stress of the cable anchor in the tier-one slope support gradually increases accordingly. There are non-linear relationships between the axial stress and the load, and the growth rate of the axial stress of the cable anchors becomes higher and higher.

#### 4.4. The change law of axial stresses of cable anchors for the joint support

Figure 19 shows the change law of cable anchors in all tiers of in-service joint supports when the slope top is under the action of  $4 \times 10^4$  N load of even distribution. Figure 20 is the cloud map of the maximum displacement of the whole slope when the evenly distributed load exerted on the slope top is  $4 \times 10^4$  N. As can be seen from Figure 19 and Figure 20, when the exertion of the evenly distributed load spawns the rise in landslide thrust, slope slide mass will slide along the sliding surface as a block; the axial stress of all cable anchors in the joint support will increase. Constrained by the joint support, the slope displacement gradually decrease from the sliding plane to the free face. The 6# cable anchor has a much faster growth rate than 4# cable anchor and 5# cable anchor. When the evenly distributed load exerted on the slope top reaches  $1 \times 10^5$  N and the maximum slope displacement is up to 25mm, the axial stresses of 1#-5# cable anchors fail to increase to the given value of prestress (800kN), but the axial stresses of 6# and 7# cable anchors already exceed 800kN. This phenomenon means that when the landslide thrust rises, it is the cable-anchor-mounted anti-slide pile and the tier-two anchor cable frame that bear most of the landslide thrust.

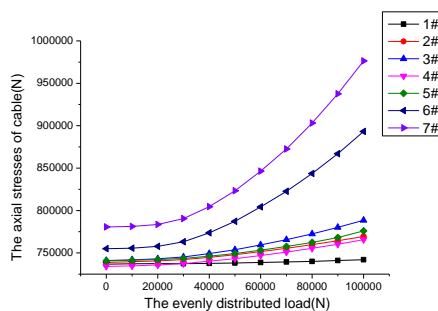


Figure 19. The axial stresses of cable anchors for all tiers of the joint support

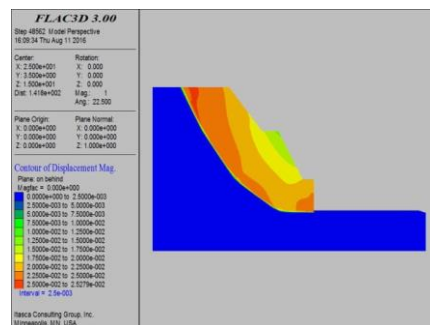


Figure 20. The cloud map of the maximum displacement of the whole slope when the evenly distributed load exerted on the slope top is  $1 \times 10^5$  N

## **Conclusion**

- 1) When evenly distributed load is exerted on the top of a slope with in-service joint support, slope slide mass will slide along the sliding surface as a block.
- 2) The tier-three slope and the frame beam will rotate counterclockwise during their sliding process. When the evenly distributed load exceeds a certain value, the growth rate of 3# cable anchor is higher than that of 2# cable anchor, and the 1# cable anchor has the lowest growth rate among them.
- 3) When landslide thrust changes as the slope top is under the action of evenly distributed loads, it is the cable-anchor-mounted anti-slide pile and the tier-two anchor cable frame that bear most of the landslide thrust.

## **Acknowledgements:**

I would like to express extend my sincere gratitude to all those who helped me during the writing of this paper, especially my mentor, professor Hai-qing Zhou, for his constant encouragement and guidance. He has walked me through all the stages of the writing of this article. Without his consistent and illuminating instruction, this article could not have reached its present form. In addition, I would like to thanks to my school Logistical Engineering University for providing the study environment for me.

The work was funded by the national natural science foundation of China (Grant No.41072243 and 41272356), the graduate student research innovation project of Chongqing.(Grant No.CYS16237)

## **References**

1. Xiao Shi-guo,Zhou De-pei. A calculation method for internal force of pre-stressed anchor-rope and frame beam-on-foundation on high rock slope[J]. Chinese Journal of Geotechnical Engineering, 2002, 24(4):479-482.
2. Wu Li-zhou, Huang Run-qiu. Numerical simulation and optimum design of anchor frame beam strengthening expansive soil road cut slope[J]. Rock and Soil Mechanics, 2006, 27(4):605-614.
3. Zheng Ming-xin, Jiang Xin-long, Yin Zong-ze, et al. Evaluation of effectiveness of pre-stressed anti-slide cable piles by numerical simulations[J]. Rock and Soil Mechanics, 2007, 28(7):1381-1386.
4. Li Peng-ju, Zhou Hai-qing, Wu Run-ze, et al. The dynamic prospecting technology and numerical simulation of landslide based on the process of construction of U type steel sheet pile[J]. Journal of Logistical Engineering University, 2014, 30(2):8-12.

5. Wu Run-ze, Zhou Hai-qing, Hu Yuan, et al. Research on distribution law of landslide thrust of anchored anti-slide pile based on FLAC3D[J]. Journal of Disaster Prevention and Mitigation Engineering, 2013, 33(5):548-555.
6. Zhang Ai-jun, Mo Hai-hong, Zhu Zhen-de, et al. Analytical solution to interaction between passive piles and soils[J]. Chinese Journal of Geo-technical Engineering, 2011, 33(Sup. 2):120-127.
7. Sun Shu-wei, Zhu Ben-zhen, Ma Hui-min. Model experimental research on anti-sliding characteristics of micropiles with cap beam[J]. Chinese Journal of Rock Mechanics and Engineering, 2010, 29(Sup.1): 3039-3044.
8. Wang Cheng, Shi Shao-qing, Chu Zhao-jun, et al. Model test of anti-slide piles soil arch effect based on the mutability of normal stress[J]. Journal of Logistical Engineering University, 2016, 32(1):1-6.
9. Wu Run-ze, Zhou Hai-qing, Hu Yuan, et al. An improved method for calculating anti-sliding pile with prestressed anchor cable based on finite difference theory[J]. Rock and Soil Mechanics, 2015, 36(6):1791-1800.
10. Zhao Ming-hua, Liao Bin-bin, Liu Si-si. Calculation of anti-slide piles spacing based on soil arching effect[J]. Rock and Soil Mechanics, 2010, 31(4):1211-1216.
11. Lei Guo-ping, Tang Hui-ming, Cheng Hao, et al. Internal force calculation of anti-slide pile socketed segment considering vertical frictional resistance[J]. Rock and Soil Mechanics, 2014, 35(8):2197-2204.
12. Lai Jie, Zheng Ying-ren, Liu Yun, et al. Shaking table test study on anti-slide piles and anchor bars of slope under earthquake[J]. China Civil Engineering Journal, 2015, 48(9):96-103.
13. Reese L C. Analysis of laterally loaded piles in weak rock[J]. Journal of Geotechnical and Geo-environmental Engineering, 1997, 123(11):1010-1017.
14. Rollins K M, Peterson K T, Weaver T Z. Lateral load behavior of full-scale pile group in clay[J]. Journal of Geotechnical and Geo-environmental Engineering, 1998, 24(6):468-478
15. Su Hang, Zhou Hai-qing, Li Peng-ju, et al. Research on construction effect of rock soil slope based on FLAC3D[J]. Journal of Logistical Engineering University, 2014, 30(6):1-6.
16. Huayou Liang, Haiqing Zhou, Hang Su, et al. The Numerical Simulation about the "overlapping effect of influence zone" of the construction process of Multi-stage slope[J]. International Journal of Earth Science and Eengineering, 2016, 09(02):848-854.